Open Archive Toulouse Archive Ouverte

Open Archive TOULOUSE Archive Ouverte (OATAO)

OATAO is an open access repository that collects the work of Toulouse researchers and makes it freely available over the web where possible.

This is an author-deposited version published in : http://oatao.univ-toulouse.fr/
Eprints ID : 11453

To link to this article : doi:10.1017/jfm.2014.145
URL : http://dx.doi.org/10.1017/jfm.2014.145

To cite this version : Izard, Edouard and Bonometti, Thomas and Lacaze, Laurent *Modelling the dynamics of a sphere approaching and bouncing on a wall in a viscous fluid.* (2014) Journal of Fluid Mechanics, vol. 747 . pp. 422-446. ISSN 1469-7645

Any correspondance concerning this service should be sent to the repository administrator: staff-oatao@listes-diff.inp-toulouse.fr

Modelling the dynamics of a sphere approaching and bouncing on a wall in a viscous fluid

Edouard Izard, Thomas Bonometti and Laurent Lacaze†

Université de Toulouse; INPT, UPS; IMFT (Institut de Mécanique des Fluides de Toulouse),
Allée Camille Soula, F-31400 Toulouse, France

CNRS; IMFT, F-31400 Toulouse, France

The canonical configuration of a solid particle bouncing on a wall in a viscous fluid is considered here, focusing on rough particles as encountered in most of the laboratory experiments or applications. In that case, the particle deformation is not expected to be significant prior to solid contact. An immersed boundary method (IBM) allowing the fluid flow around the solid particle to be numerically described is combined with a discrete element method (DEM) in order to numerically investigate the dynamics of the system. Particular attention is paid to modelling the lubrication force added in the discrete element method, which is not captured by the fluid solver at very small scale. Specifically, the proposed numerical model accounts for the surface roughness of real particles through an effective roughness length in the contact model, and considers that the time scale of the contact is small compared to that of the fluid. The present coupled method is shown to quantitatively reproduce available experimental data and in particular is in very good agreement with recent measurement of the dynamics of a particle approaching very close to a wall in the viscous regime $St \leqslant O(10)$, where St is the Stokes number which represents the balance between particle inertia and viscous dissipation. Finally, based on the reliability of the numerical results, two predictive models are proposed, namely for the dynamics of the particle close to the wall and the effective coefficient of restitution. Both models use the effective roughness height and assume the particle remains rigid prior to solid contact. They are shown to be pertinent to describe experimental and numerical data for the whole range of investigated parameters.

Key words: computational method, lubrication theory, particle/fluid flow

1. Introduction

Immersed granular and particle-laden flows are encountered in a large number of industrial and natural applications, including chemical engineering, aeronautics, transportation, biomechanics, geophysics and oceanography. Granular flows with negligible effect of the surrounding fluid are gravity-driven and dissipated by inelastic and frictional contacts, while when the effect of the fluid becomes non-negligible, the hydrodynamic forces can drive the particle motion and the bulk kinetic energy may be

† Email address for correspondence: lacaze@imft.fr

additionally dissipated by viscous effects. In addition, such flows may exhibit strong inhomogeneities in the spatial distribution of particle velocity and concentration. To understand the dynamics of such complex systems, an accurate description of the dynamics at the particle scale for a large range of particle Reynolds number and Stokes number is needed (the Stokes number being the ratio of the relaxation time of the particle to the characteristic time scale of the fluid). For example, in a shear-driven immersed granular flow encountered in natural flows, some particles located at depth in the bed are quasi-stationary while others, at the bed surface, can reptate, salt or get entrained as a suspension in the bulk. This large range of dynamical parameters makes the development of predictive models very difficult. It is therefore necessary to improve the local description of canonical configurations in which processes can be isolated. In particular, the description of a single bounce of a particle in a fluid at rest remains challenging. Here we are interested in this configuration, namely the bouncing of a spheroidal particle on a wall in a viscous fluid.

Experiments on binary collisions in fluid have been undertaken in many studies. In a first approach, the collision of a particle on a wall covered by a thin liquid film has been experimentally investigated in order to highlight the lubrication effect on the bouncing (Barnocky & Davis 1988; Lundberg & Shen 1992). More generally, the case of a fully immersed system has been investigated (Joseph *et al.* 2001; Gondret, Lance & Petit 2002; Ten Cate *et al.* 2002; Pianet *et al.* 2007; Mongruel *et al.* 2010). In this case, the dynamics is slightly more complex since unsteady drag and history force can affect the falling of the particle well before the influence of the lubrication. In any case, the specific effect of the presence of the fluid is to take part in the dissipation of the initial kinetic energy leading to a decrease of the apparent coefficient of restitution of the bouncing particle. It has been shown that a similar trend is observed for two impacting particles (Yang & Hunt 2006).

The extension to the oblique bouncing on a wall in a fluid has been experimentally investigated by Joseph & Hunt (2004), the aim being to highlight the effect of lubrication on the apparent coefficient of friction. In particular, they showed that the value of the coefficient of friction, compared to the dry case, has more of an affect for smooth surfaces for which deformation induced by hydrodynamic pressure prior to solid interaction is more likely to happen. As noted by Joseph & Hunt (2004), the latter phenomenon is not observed for glass spheres and hence not expected for 'rough' particles, as long as the ratio between roughness height and particle diameter is not too small.

All these experiments agreed on the dependence of the coefficient of restitution $\varepsilon = -V_R/V_T$, defined as the ratio between the terminal velocity V_T prior to impact and the rebound velocity V_R, on the Stokes number based on the terminal velocity V_T, defined by $St = \rho_p V_T D/9\mu$ where D and ρ_p are the diameter and the density of the particle, respectively, and μ is the dynamic viscosity of the surrounding fluid. For impact at high Stokes number, $St > 2000$, the viscous dissipation does not affect the rebound of the particle much and the effective coefficient of restitution approaches that of the dry case ε_{max}. At low St, viscous damping becomes more important leading to $\varepsilon < \varepsilon_{max}$. A critical particle Stokes number $St_c \approx 10$ is experimentally observed below which no rebound occurs. The high-St trend explains the choice of a normalized coefficient of restitution $\varepsilon/\varepsilon_{max}$ usually found in the literature.

Models of binary interaction of solid particles have been widely developed in the literature and can be divided into two main contributions: one concerning the dynamics of the approaching solid and the second concerning the modelling of an effective coefficient of restitution after bouncing.

Brenner ([1961](#)) gives an analytic expression for the repulsive force acting on a smooth rigid sphere approaching a wall at low Reynolds number. When considering an elastic solid, this force is affected by the deformation of the material. Theoretical studies of elasto-hydrodynamic (EHD) collision of two spheres in a liquid showed through asymptotic and numerical techniques the relation between the pressure induced by lubrication and the deformation of the particle. These works were a first attempt to predict if a solid particle can bounce or if it, rather, sticks to the wall (Davis, Serayssol & Hinch [1986](#); Barnocky & Davis [1989](#)). The influence of particle roughness was introduced by Smart & Leighton ([1989](#)) who show that it plays an important role in the contact dynamics. In particular, they highlight the fact that, during bouncing, the characteristic length of the fluid layer is of the same order of magnitude as the roughness height. Several studies have been devoted to understanding and modelling the influence of the roughness during bouncing or prior to contact. For instance, Lecoq *et al.* ([2004](#)) found that the dynamics of a particle approaching a rough wall is similar to the case of an equivalent smooth wall slightly shifted away from the original upper position of the corrugated surface.

Global models have also emerged for predicting the bouncing via the effective coefficient of restitution ε as a function of the Stokes number. For instance, Lian, Adams & Thornton ([1996](#)) extend the EHD theory, using a Hertz-like model for the elastic deformation to predict the coefficient of restitution. The proposed model agrees with numerical solutions of the system of equations but needs a scaling coefficient to obtain a closed-form solution. Legendre, Daniel & Guiraud ([2005](#)) derived a model for bouncing drops on a solid wall, using a mass–spring analogy accounting for the deformation of the drop. This model has proved successful and has been shown to reproduce the case of bouncing solid particles by adjusting an empirical constant. More recently, the effective coefficient of restitution ε has been modelled with a mixed contact model (Yang & Hunt [2006](#), [2008](#)), for which St_c and a scaled surface roughness have to be prescribed.

In the present study, a coupled fluid–solid method is developed to investigate the bouncing of a solid particle on a horizontal bottom wall. Simulating solid–fluid interaction is often difficult because of the complexity of the solid shape and motion in the fluid flow. Methods for modelling solid–fluid interaction may be divided into two main groups, depending on the way the solid–fluid interfaces are described. One group, usually referred to as body-fitted grid methods, makes use of a structured curvilinear or unstructured grid to conform the grid to the boundary of the fluid domain (see e.g. Thompson, Warsi & Mastin [1985](#)). In situations involving complex moving boundaries, one needs to establish a new body-conformal grid at each time-step which leads to a substantial computational cost and subsequent slowdown of the solution procedure. In addition, issues associated with regridding arise such as grid-quality and grid-interpolation errors. The second group of methods is referred to as fixed-grid methods. These techniques make use of a fixed grid, which eliminates the need for regridding, while the presence of the solid objects is taken into account via adequately formulated source terms added to fluid flow equations. Fixed-grid methods have emerged in recent years as a viable alternative to body-conformal grid methods. In this group, one can mention the immersed boundary method (IBM) (Fadlun *et al.* [2000](#); Kim, Kim & Choi [2001](#); Peskin [2002](#); Uhlmann [2005](#); Feng, Michaelides & Mao [2010](#); Breugem [2012](#); Kempe & Fröhlich [2012](#); Li, Hunt & Colonius [2012](#)), distributed Lagrangian multiplier-based methods (Ardekani & Rangel [2008](#)) or tensorial penalty methods (Brändle de Motta *et al.* [2013](#)), among others.

In the present work, we attempt to simulate the local dynamics of such systems at the particle scale by simulating the collision of a sphere with a wall. To this end a

simple soft-sphere collision IBM is presented. The IBM consists of a direct forcing method, using a continuous solid volume fraction to define the boundary. The granular medium is modelled with a discrete element method (DEM) based on a multi-contact soft-sphere approach.

The paper is structured as follows. First, we describe the numerical technique used here. Secondly, wall–particle collisions in a fluid are simulated for a wide range of Stokes number ranging from 1 to 10^4, and the use of a local lubrication force is discussed. Then, the dynamics of the particle approaching a wall at low Stokes number is simulated with IBM–DEM and compared to experimental data. The extension of an existing model (Mongruel *et al.* 2010) is proposed with, in particular, the implementation of an effective roughness length. Finally, a new model predicting the effective coefficient of restitution as a function of the Stokes number and the relative roughness height of the particles is proposed.

2. Numerical approach

2.1. *Calculation of the fluid flow*

The fluid flow around the particle is obtained thanks to an IBM. Assuming a Newtonian fluid, the evolution of the flow is described using the Navier–Stokes equations, namely

$$\nabla \cdot V = 0, \tag{2.1}$$

$$\frac{\partial V}{\partial t} + \nabla \cdot (V \otimes V) = g - \frac{1}{\rho}\nabla P + \frac{1}{\rho}\nabla \cdot \left[\mu \left(\nabla V + {}^t\nabla V \right) \right] + f, \tag{2.2}$$

where V, P, ρ and μ are the local velocity, pressure, density and dynamic viscosity in the fluid, respectively, g denotes acceleration due to gravity and f is a body-force source term used to take into account solid–fluid interaction. Equations (2.1) and (2.2) are written in a Cartesian or polar system of coordinates. These equations are enforced throughout the entire domain, comprising the actual fluid domain and the space occupied by the particles. In the following, the term f will be formulated in such a way as to represent the action of the immersed solid upon the fluid. Let us consider a solid particle of density ρ_p, volume $\mathcal{V}_p$ and mass m_p, the centroid of which being located at x_p, moving at linear and angular velocity u_p and ω_p, respectively. The local velocity U of the solid object is then defined by $U = u_p + r \times \omega_p$, r being the local position relative to the solid centroid.

The time integration of the momentum equation for the fluid (2.2) is performed via a third-order Runge–Kutta method for all terms except the viscous term for which a second-order semi-implicit Crank–Nicolson scheme is used. The incompressibility condition (2.1) is satisfied at the end of each time step through a projection method. Domain decomposition and message passing interface (MPI) parallelization is performed to facilitate simulation of a large number of grid cells. In general, the location of the particle surface is unlikely to coincide with the grid nodes, so that interpolation techniques are usually employed to enforce the boundary condition by imposing constraints on the neighbouring grid nodes. Here we adopt another strategy, by introducing a function α, which denotes solid volume fraction, which is equal to one in cells filled with the solid phase, zero in cells filled with the fluid phase, and $0 < \alpha < 1$ in the region of the boundary. In practice, the transition region is set up to be of 1–3 grid cells approximately (Yuki, Takeuchi & Kajishima 2007). The forcing term is

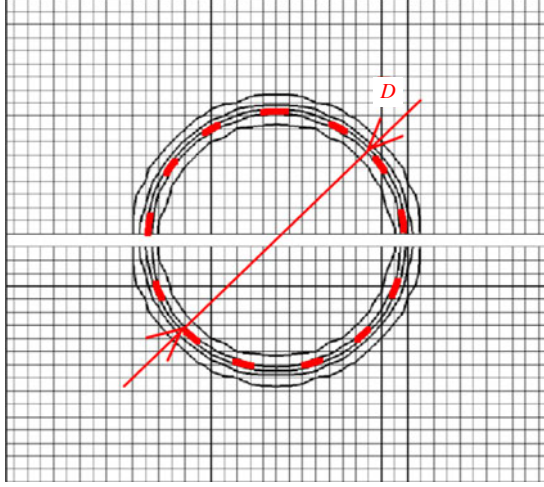$$f = \alpha \frac{U - V}{\Delta t}. \tag{2.3}$$

FIGURE 1. (Colour online) Example of the grid used in the present immersed-boundary simulation. Iso-contours of $\alpha = 0.01$, 0.25, 0.5, 0.75 and 0.99. Here $D/\Delta x \approx 20$ with D the diameter of the solid particle considered. The dashed line shows the contour of the solid particle which is used in the DEM code.

Recall that U is the local velocity imposed on the immersed solid object while V is the local velocity in the fluid; Δt is the time step used for the time-advancement. The present choice, which may be viewed as a smoothing of the immersed boundary, is an alternative to using a regularized delta function in conjunction with a Lagrangian marking of the boundary. The latter technique is largely used in IBMs in order to allow a smooth transfer of momentum from the boundary to the fluid (see e.g. Fadlun *et al.* 2000; Uhlmann 2005). The present approach is simple to implement and does not need any Lagrangian mesh for tracking the immersed boundary. In the following, spherical particles are considered. The corresponding solid volume fraction α is defined by

$$\alpha(\boldsymbol{x}) = \frac{1}{2} - \frac{1}{2}\tanh\left(\frac{|\boldsymbol{x} - \boldsymbol{x}_p| - R}{\lambda\phi\Delta}\right), \tag{2.4}$$

$$\lambda = |n_x| + |n_y| + |n_z|, \tag{2.5}$$

$$\phi = 0.065(1 - \lambda^2) + 0.039, \tag{2.6}$$

where $\boldsymbol{n} = (n_x, n_y, n_z)$ is a normal outward unit vector at a surface element, R is particle radius, ϕ is a parameter controlling the thickness of the transition region and Δ is a characteristic grid size ($\Delta = \sqrt{2}\Delta x$ when the grid is uniform). Note that the coefficients used in (2.6) are 1.3 times larger than those reported in Yuki *et al.* (2007). This choice stems from numerical tests on moving cylinders at moderate Reynolds number which showed that the present set of coefficients is sufficient to suppress parasitic fluctuations of the forces applied to the objects when the latter cross a numerical cell (not shown here). The reader is referred to Uhlmann (2005) for a detailed discussion of this point. Iso-contours of α as defined in (2.4) for a solid particle of diameter D are shown in figure 1. In this case, the transition region is of three grid cells approximately.

2.2. *Calculation of the particle motion*

The motion of the particle is described by Newton's equations for linear and angular momentum of a rigid body, namely

$$m_p \frac{\mathrm{d}\boldsymbol{u}_p}{\mathrm{d}t} = m_p \boldsymbol{g} + \boldsymbol{F}_h + \boldsymbol{F}_c + \boldsymbol{F}_{lub}, \quad \boldsymbol{I}_p \frac{\mathrm{d}\boldsymbol{\omega}_p}{\mathrm{d}t} = \boldsymbol{\Gamma}_h + \boldsymbol{\Gamma}_c, \quad (2.7a,b)$$

where $\boldsymbol{F}_h$ (resp. $\boldsymbol{\Gamma}_h$) is the hydrodynamic force (resp. torque) defined by

$$\boldsymbol{F}_h = -\frac{\rho\rho_p}{\rho_p - \rho} \int_{\mathcal{V}_p} \boldsymbol{f} \mathrm{d}V, \quad \boldsymbol{\Gamma}_h = -\frac{\rho\rho_p}{\rho_p - \rho} \int_{\mathcal{V}_p} \boldsymbol{r} \times \boldsymbol{f} \mathrm{d}V. \quad (2.8a,b)$$

Equation (2.8) was derived by Uhlmann (2005) or Bigot *et al.* (2013) for instance, and will not be repeated in detail here. Briefly, (2.8) are derived by integrating the momentum law (2.2) and corresponding kinematic momentum law for the fluid on the volume of the immersed object, and ensuring that the fictitious body force $\boldsymbol{f}$ is such that these integrated laws are equivalent to the Newton equations (2.7). In (2.7), $\boldsymbol{F}_c$ (resp. $\boldsymbol{\Gamma}_c$) is the contact force (resp. torque) including particle–particle and particle–wall collisions, and $\boldsymbol{F}_{lub}$ is a lubrication force. A detailed description of these forces is given in §§ 2.2.1 and 2.2.2, respectively. In the case of multiple solid objects moving in a fluid, it is known that when the distance between two objects is small enough, the lubrication force induced by the interstitial flow becomes the dominant force in (2.7). Depending on the properties of the fluid and the relative velocity between the objects, the characteristic length of influence can be several orders of magnitude smaller than the particle diameter (Joseph *et al.* 2001). The present fixed-grid method described in the previous section is then unable to accurately capture the lubrication force for a reasonable grid resolution. Moreover, in the case of a perfectly smooth object, $\boldsymbol{F}_{lub}$ diverges as the inverse of the distance between particles goes to zero, therefore avoiding any possible interaction between particles. The latter phenomenon does not consider surface roughness of real particles allowing solid contact as explained in Smart & Leighton (1989). Modelling these short-range interactions, both the lubrication and solid contact, is therefore crucial to capture the small-scale physics of solid particles interacting in a fluid.

In the present study, the small-scale interaction is modelled using a soft-sphere discrete element method (DEM) solving (2.7). This method has been developed to allow multi-contact interactions for a large number of particles, but is used here to consider the simpler case of a single contact between a solid sphere and a wall.

Length scales and time scales associated with short-range interactions are small compared to those associated with the fluid flow. The coupling between IBM and DEM is therefore done by solving (2.7) using a time step which is at least two orders of magnitude smaller than the fluid time step used to solve (2.1) and (2.2). In other words, large-scale flow structures (of the order of the particle size or larger) computed with the IBM approach are frozen during the computation of short-range interactions with the DEM code. Such a numerical trick allows to reduce computational cost which would have been tremendous if we had reduced the time step of the IBM down to the time step imposed by the DEM resolution. It has been verified that changing the ratio between the two time steps in the range 10^2–10^3 does not affect the results.
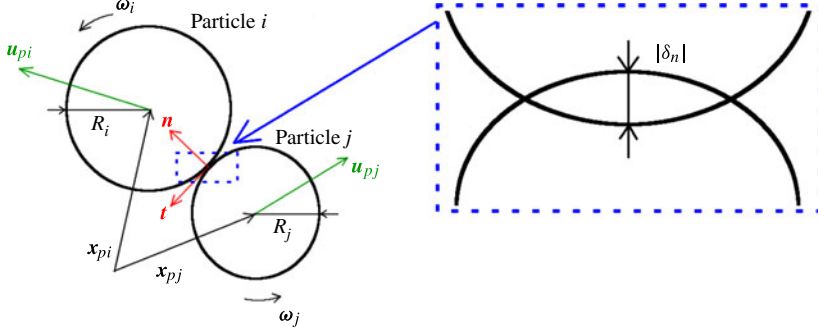
FIGURE 2. (Colour online) Sketch of a contact in the DEM soft-sphere model with the associated notation; δ_n is the normal signed distance of overlap defined as $\delta_n = \|\boldsymbol{x}_{pi} - \boldsymbol{x}_{pj}\| - (R_i + R_j)$.

2.2.1. *Solid contact modelling*

Here, we describe the method used for dealing with solid contacts in a system of n_p particles for generality. The modelling of the solid–solid interaction is done via a soft-sphere approach (Cundall & Strack 1979), which is based on modelling the deformation of real particles during contact by an overlap between computed non-deformable particles (figure 2). This overlap is then used to compute the normal and tangential contact forces, using here a linear mass–spring system and a Coulomb-type threshold for the tangential component, in order to account for solid sliding. The force $\boldsymbol{F}_c$ and the torque $\boldsymbol{\Gamma}_c$ are decomposed such that

$$\boldsymbol{F}_c = \sum_{j \neq i} \boldsymbol{F}_{ij} + \boldsymbol{F}_{wall}, \tag{2.9}$$

$$\boldsymbol{\Gamma}_c = \sum_{j \neq i} \boldsymbol{\Gamma}_{ij} + \boldsymbol{\Gamma}_{wall}, \tag{2.10}$$

where $\boldsymbol{F}_{ij}$ is the contact force between particles i and j, $\boldsymbol{F}_{wall}$ the wall–particle interaction force; $\boldsymbol{\Gamma}_{ij}$ and $\boldsymbol{\Gamma}_{wall}$ are the corresponding torques. $\boldsymbol{F}_{ij}$ and $\boldsymbol{\Gamma}_{ij}$ are computed using a local system of coordinates $(\boldsymbol{n}, \boldsymbol{t})$, depicted in figure 2, as follows:

$$\boldsymbol{F}_{ij} = F_n \boldsymbol{n} + F_t \boldsymbol{t}, \tag{2.11}$$
$$\boldsymbol{\Gamma}_{ij} = R_i \boldsymbol{n} \times F_t \boldsymbol{t}, \tag{2.12}$$

with

$$F_n = \begin{cases} 0 & \text{if } \delta_n > 0 \\ \max\left(0, -k_n \delta_n - \gamma_n \dfrac{d\delta_n}{dt}\right) & \text{otherwise.} \end{cases} \tag{2.13}$$

$$F_t = -\min(|k_t \delta_t|, |\mu_c F_n|)\mathrm{sign}(\delta_t), \tag{2.14}$$

where R_i is the ith particle radius, δ_n (δ_t) is the normal (tangential) signed distance of overlap, μ_c is the friction coefficient, k_n (k_t) is the normal (tangential) stiffness and γ_n is the damping coefficient of the mass–spring model. Here, δ_t is obtained by

integrating the following equation between the time at which contact occurs and the current time:

$$\frac{\mathrm{d}\delta_t}{\mathrm{d}t} = (\boldsymbol{u}_{pi} - \boldsymbol{u}_{pj}) \cdot \boldsymbol{t}. \tag{2.15}$$

Note that $\boldsymbol{F}_{wall}$ and $\boldsymbol{\Gamma}_{wall}$ are treated in a similar manner by taking an infinite radius and mass for the wall. The constants of the mass–spring model, γ_n, k_n and k_t, are calculated thanks to two additional parameters, namely the coefficient of normal restitution ε_{max} and the contact time t_c which are characteristic of the elastic properties of the particles, namely

$$\gamma_n = -\frac{2m_*}{t_c} \ln(\varepsilon_{max}), \tag{2.16}$$

$$k_n = \frac{m_* \pi^2}{t_c^2} + \frac{\gamma_n^2}{4m_*}, \tag{2.17}$$

where $m_* = (m_i m_j)/(m_i + m_j)$ is the effective mass involved in the contact. Note that the relation (2.17) between the contact time and the material stiffness is not that predicted by Hertz theory. This is due to the present linear model used for calculating the normal contact force (see e.g. Schäfer, Dippel & Wolf 1996). Moreover, deducing k_n from t_c is somewhat unusual since k_n is related to the stiffness of the considered material. However, it has been shown in numerous studies (see Lacaze, Phillips & Kerswell 2008, for instance) that k_n can be underestimated without modification of the dynamics of a dry system. It allows reduction of the execution time of the simulation. For practical reasons of coupling with the fluid, we decide to fix t_c, verifying that the value of k_n is large enough to consider the particles as hard. In the case of quasi-mono-disperse configurations, it can be shown that choosing k_n as a function of t_c and vice versa is equivalent since properties of particles are the same. Finally, the tangential stiffness coefficient k_t is assumed to be proportional to the normal stiffness coefficient k_n (Foerster *et al.* 1994). In the present work, we set $k_t = 0.2k_n$. Details of the DEM code and validations in the case of multi-particle configurations will be given in a future paper. In the present case, only the normal binary interaction between a particle and a wall is considered in detail since the coupling with a fluid solver still needs some specific attention.

2.2.2. *Lubrication force modelling*

As will be shown in §3.1, the IBM may not be accurate in capturing the detailed flow structure in the liquid film which is drained when the particles approach each other, if the spatial resolution used to resolve the flow in the narrow gap is too low. This can be overcome by locally refining the grid resolution in the liquid film, as done in Ardekani & Rangel (2008) for instance. However, this strategy becomes inefficient when multiple contacts (of the order of 10^3 or more) occur in the system and even more in three-dimensional situations. Another strategy is to add a lubrication force $\boldsymbol{F}_{lub}$ in (2.7) (Ten Cate *et al.* 2002; Breugem 2010; Kempe & Fröhlich 2012; Simeonov & Calantoni 2012; Brändle de Motta *et al.* 2013). Here, only the normal component of the lubrication force is considered. It should be noted that even in the case of tangential interaction, Kempe & Fröhlich (2012) have shown that the tangential component of lubrication does not affect significantly the dynamics of two

interacting objects. The lubrication force used here between particle i and particle j of velocity $\boldsymbol{u}_{pi}$ and $\boldsymbol{u}_{pj}$ and radius R_i and R_j, respectively, is (Brenner 1961)

$$\boldsymbol{F}_{lub} = -\frac{6\pi\mu(\boldsymbol{u}_{pi}\cdot\boldsymbol{n} - \boldsymbol{u}_{pj}\cdot\boldsymbol{n})}{\delta_n + \eta_e} \left(\frac{R_i R_j}{R_i + R_j}\right)^2 \boldsymbol{n}, \tag{2.18}$$

where η_e stands for an effective roughness height accounting for the mean height of surface asperities of real particles η. This parameter is added to (2.18) in order to mimic real particles and avoid the divergence of the force when contact occurs ($\delta_n = 0$). Depending on the type of material used for the particles, the relative mean height of surface asperities η/R is roughly in the range $[10^{-6}; 10^{-3}]$ (Joseph *et al.* 2001). In the following, the same range of values of η_e/R is used. It should be noted that the conversion from η to η_e is not trivial and η_e is therefore considered as a way of modelling the microscopic structure of the particle surface. It is however reasonable to assume that its order of magnitude is related to the real roughness, as a first approximation. The reader is referred to Mongruel *et al.* (2013) for a detailed discussion of this point.

The definition (2.18) using η_e is motivated by observations of Davis (1987) who shows that the presence of surface roughness does not affect the lubrication force until the gap between surfaces is of the same order of magnitude as the mean height of surface asperities η. The standard lubrication model obtained for perfectly smooth surfaces therefore still holds. In addition, Lecoq *et al.* (2004) show that surface roughness indeed affects contact equivalently to if it were a smooth contact for which lubrication is only shifted by a length of the order of the roughness height. Again, this is in line with the definition of (2.18).

In the case of particles interacting with a horizontal wall, as considered here, the lubrication force remains similar to (2.18) but setting the radius to infinity for the wall. The present lubrication force is switched on when the distance between particles is such as $0 \leqslant \delta_n \leqslant R/2$. This upper bound is in the range of the critical distance h_w at which the velocity of the particle decreases due to the presence of the wall that was measured in the experiments of Joseph *et al.* (2001), namely $0 \leqslant h_w \leqslant R$ for $9 \leqslant St \leqslant 70$ (see their figure 10). We checked that the specific value of the upper bound of the force application (within the range $[\Delta x; R]$) did not affect the results significantly (figure 6a and table 2).

3. Bouncing of a solid sphere on a wall in a viscous fluid

3.1. *Dynamics of the bouncing particle and effective coefficient of restitution*

The dynamics of a spherical particle of radius R and density ρ_p, released in a viscous liquid initially at rest, sedimenting and then bouncing on a wall, is considered here. To this end, the coupled equations (2.1)–(2.7) are solved, as described in the previous section. In the range of physical parameters considered here, the fluid flow generated by the falling particle is axisymmetric, hence the fluid flow is solved on a two-dimensional axisymmetric grid. The simulation is performed on an (r,z)-domain of size $10.4D \times 44D$, D being the particle diameter, with 80×880 grid points. The spatial resolution is constant along the z direction parallel to gravity as well as in the region $0 \leqslant r/D \leqslant 2.5$ ($D/\Delta x = 20$). For $2.5 \leqslant r/D \leqslant 10.4$, the grid size is varied following an arithmetic progression up to the outer wall. Note that the grid resolution is similar to the one shown in figure 1, corresponding to $D/\Delta x = 20$. Simulations with $D/\Delta x = 10$ and 40 have been performed and showed that the spatial resolution

does not affect the results (figure 6 and table 2). Free-slip boundary conditions are imposed at all boundaries except at the bottom wall where bouncing occurs for which a no-slip condition is applied. The particle is initially located at a distance of $4D$ from the upper wall in order to ensure that the particle reaches a constant terminal velocity V_T before being influenced by the wall.

The dynamics of a sedimenting particle depends on two dimensionless parameters which can be computed *a priori*, namely the density ratio ρ_p/ρ and the Archimedes number $Ar = \rho(\rho_p - \rho)gD^3/\mu^2$, ρ and μ being the fluid density and viscosity, respectively. We set the physical properties of the particle and the fluid so that we cover a large range of density ratios $1.7 \leqslant \rho_p/\rho \leqslant 10^3$ and Archimedes numbers $10 \leqslant Ar \leqslant 2 \times 10^4$. These lead to *a posteriori* values of particle Reynolds numbers $10^{-1} \leqslant Re_p \leqslant 160$ and Stokes numbers $10^{-1} \leqslant St \leqslant 10^3$, being defined as

$$Re_p = \frac{\rho V_T D}{\mu}, \quad St = \frac{(\rho_p + C_M \rho)V_T D}{9\mu}, \quad (3.1a,b)$$

where $C_M = 1/2$ is the added-mass coefficient of the spherical particle. In the present simulations, the maximum Reynolds number is 163 which is $\sim 20\%$ smaller than the critical value $Re^{SO} = 212.58$ of the Reynolds number for which a freely moving sphere will lose rectilinear motion to attain an oblique path, as recently shown by Fabre, Tchoufag & Magnaudet (2012) using a weakly nonlinear stability analysis. Equivalently, the Archimedes number was less than 2.4×10^4 which is the critical value (with the present definition) below which steady vertical particle motion with full axisymmetry in the horizontal plane is observed, at all density ratios (Jenny, Dusek & Bouchet 2004). Thus the use of an axisymmetric grid is relevant here.

Note that the present definition (3.1) of the Stokes number is unusual since it accounts for the added-mass involved in the motion. This definition becomes equivalent to the classical definition, namely $St = (\rho_p/9\rho)Re$ when the density ratio ρ_p/ρ is large, as in the case of solid objects in air, but not in the case of particles or drops in liquids. In this case, Legendre *et al.* (2005) showed that the use of (3.1) allows the experimental data for drops in water to fall into the range of data for particles in air or liquids. Thus (3.1) is preferred here and will be used throughout this work.

The evolution of the vorticity field around the particle during impact is presented in figure 3, for the case $\rho_p/\rho = 8$, $Ar = 3700$ ($St \approx 53$, $Re_p \approx 60$). Here the solid contact parameters were set to $\varepsilon_{max} = 0.97$, $t_c\sqrt{g/D} = 2.5 \times 10^{-3}$, $\mu_c = 0.25$, and the relative effective roughness height used in the lubrication model (2.18) was set to $\eta_e/R = 4 \times 10^{-4}$. Snapshots of the vorticity field are presented in figure 3 at different stages of the rebound. The particle is represented by the solid volume fraction α as defined in (2.4) which is coloured in black. In this section time is scaled by $\sqrt{D/g}$. At $t = 19.74$, the flow field around the particle is not influenced by the wall and therefore corresponds to the steady-state motion of the particle settling in a viscous fluid. When the sphere gets closer to the wall (a distance of R approximately from the wall, at $t = 19.89$), the fluid is pushed away from the centreline and vorticity is created at the wall (figure 3b). Note that at this stage, the liquid film between the particle and the wall is still accurately resolved by the fluid solver. When collision occurs at $t = 20.02$ ($\delta_n \leqslant 0$), the vorticity is maximum in a region close to the impact zone, indicating strong shear stress as fluid is pushed away parallel to the wall. Once contact is over and the particle is detaching from the wall ($20.07 \leqslant t \leqslant 20.25$), vorticity of opposite sign emerges at the wall, the signature of the inward flow associated with
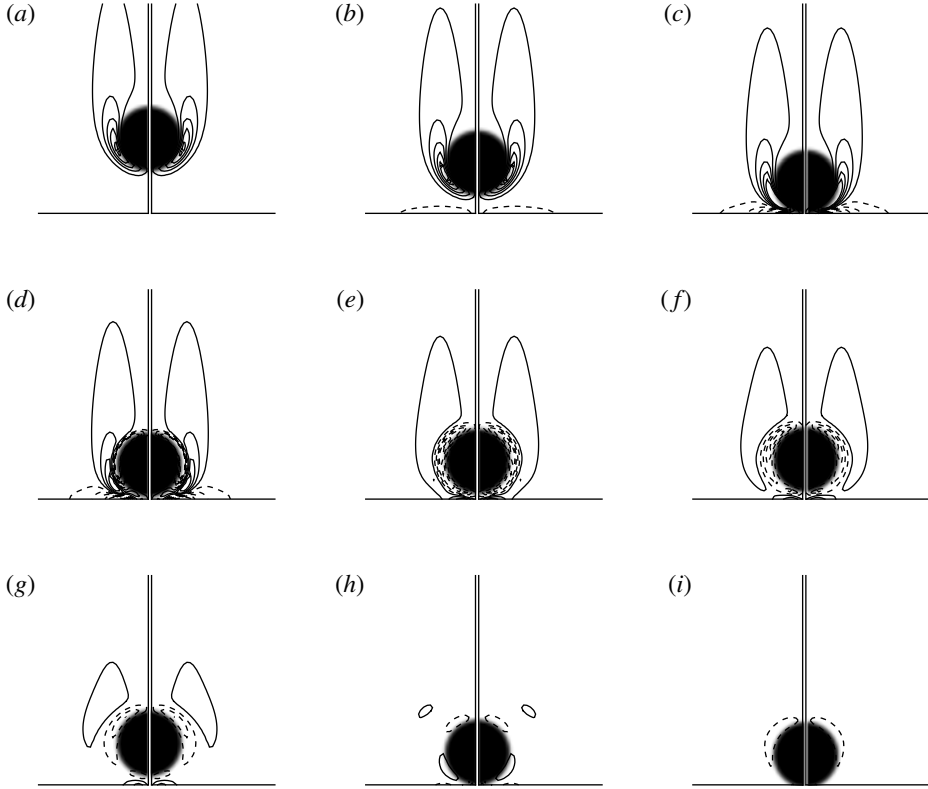
FIGURE 3. Vorticity field around a sphere impacting a wall ($\rho_p/\rho = 8$, $Ar = 3700$, $St \approx 53$, $Re_p \approx 60$, $D/\Delta x = 20$). Contours levels are set from -17.8 to 17.8 in increments of 3.9. Here, time and vorticity are scaled by $\sqrt{D/g}$ and $\sqrt{g/D}$, respectively. The vorticity field and half-particle have been mirrored for clarity. Continuous and dashed lines correspond to vorticity of opposite sign. (a) $t = 19.74$, (b) 19.89, (c) 20.02, (d) 20.07, (e) 20.17, (f) 20.25, (g) 20.48, (h) 21.06, (i) 21.27.

fluid moving back to the centreline to fill the gap between the particle and the wall. During this stage, the initial vorticity in the wake of the falling particles preceding bouncing decreases while vorticity of opposite sign appears around the particle. At $t = 20.48$, the particle has reached its maximum height after the first bouncing and falls back again toward the wall. Afterwards ($t \geqslant 21.06$), the vorticity around the particle quickly disappears because of significant viscous dissipation.

The corresponding time evolution of the particle velocity is displayed in figure 4. Clearly, the particle reaches a steady-state velocity, denoted V_T, before being influenced by the presence of the wall. It can be noted that before solid contact occurs the particle velocity decreases from V_T to an impact velocity, denoted V_C, which is $\sim 12\%$ less than V_T in the present case. During the bouncing, the particle velocity changes sign but does not recover its initial amplitude. The rebound velocity is denoted V_R, defined as the velocity 'just after' solid contact, when the particle detaches from the horizontal wall. To be more explicit, with the present approach and in the present problem, V_R is the maximum value of the velocity of sign opposite to V_T. After the impact, a strong decrease of the velocity occurs which is followed by
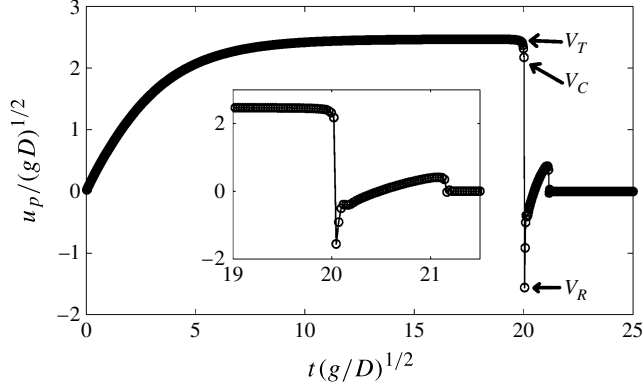
FIGURE 4. Temporal evolution of the particle vertical velocity (same case as figure 3). Inset: close-up view of the velocity during bouncing. Also defined are the particle terminal velocity V_T, the velocity at contact V_C and the rebound velocity V_R.

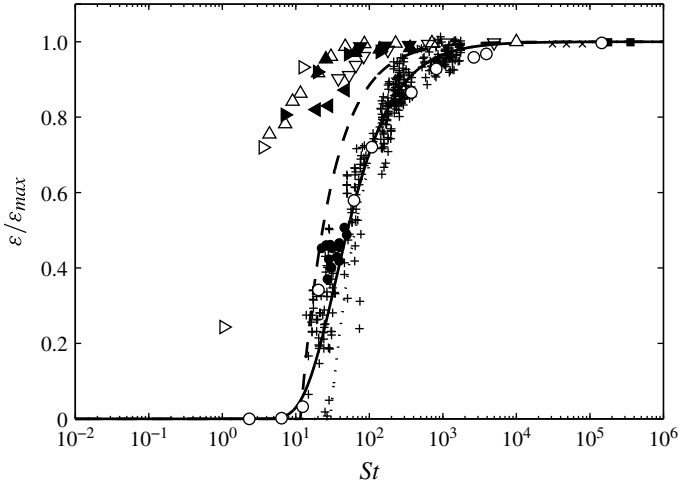
FIGURE 5. Normalized effective coefficient of restitution $\varepsilon/\varepsilon_{max}$ for spherical inclusions versus the Stokes number St. Present simulations without lubrication force: $\triangleright$, $Re_p \approx 1$; $\triangle$, $Re_p \approx 10$; $\triangledown$, $Re_p \approx 100$; $\blacktriangleleft$, $\rho_p/\rho = 2.5$; $\blacktriangleright$, $\rho_p/\rho = 8$; $\blacktriangle$, $\rho_p/\rho = 16$; $\blacktriangledown$, $\rho_p/\rho = 32$. Experiments: see table 1 for key. Analytical solutions: - - - -, prediction (3.3) with $\kappa = 1$ and $\eta/R = 10^{-4}$; $\cdots\cdots$, prediction (3.4) with $\varepsilon_{max} = 0.97$, $St_c = 20$, $\delta_f/\delta_0 = 10^{-3}$; ———, Legendre *et al.* (2005)'s correlation.

a milder trend. Finally, one can observe a second rebound ($t \approx 21$) which is hardly detectable from the flow visualization.

In the following, the simulations presented were performed for four fixed density ratios $\rho_p/\rho = 2.5$, 8, 16 and 32 (Re_p varying in the above-mentioned range) and three specific particle Reynolds numbers $Re_p = 1$, 10 and 100 (ρ_p/ρ and Ar varying in the above-mentioned range). In the different cases, the Stokes number covers a range of values within the interval $[10^{-1}, 10^3]$. These simulations were performed without a lubrication model (figure 5) and with the lubrication model (2.18) for different cases (figure 6). A classical observable quantity extracted from the rebound of a
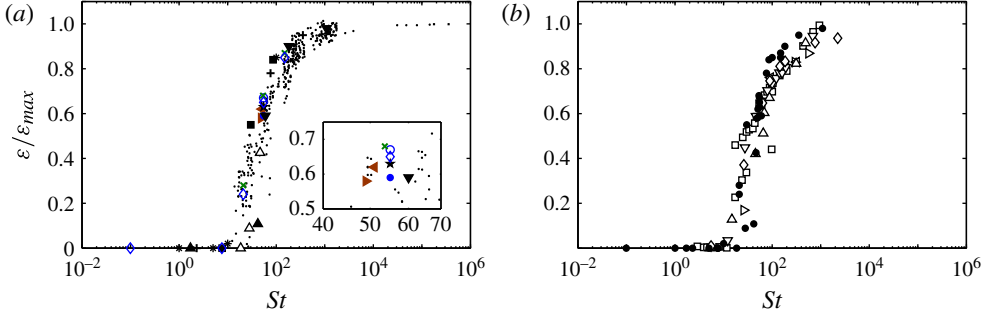
FIGURE 6. (Colour online) Normalized effective coefficient of restitution versus the Stokes number obtained with the present simulations using the lubrication force (2.18). Comparison with (*a*) the same experimental data as figure 5 here represented by dots for clarity (see table 2 for key), and (*b*) available computation data (see table 3 for key).

	Reference	Type of object	Ambient fluid
○	Gondret *et al.* (2002)	Solid	Glycerol–water
+	Joseph *et al.* (2001)	sphere	mixture
×	Foerster *et al.* (1994)	Solid sphere	Air
•	Legendre *et al.* (2005)	Toluen drop	Water
♦	Richard & Quéré (2000)	Liquid drop	Air
■	Richard & Quéré (2000)	Spherical balloon	Glycerol–water

TABLE 1. Experimental data used in figures 5, 6(*a*) and 10.

particle in a viscous fluid is the effective coefficient of restitution ε, which has been shown to depend on the mechanical properties of the particle and the Stokes number (see Gondret *et al.* 2002, for instance). It should be noted that when the fluid does not influence the dynamics and subsequent rebound of the particle, the bouncing process is referred to as a 'dry collision'. In such a case, the effective coefficient of restitution ε is maximum and equal to the 'dry coefficient of restitution' ε_{max}, the latter corresponding to a solid impact between the particle and the wall.

Here, we define the effective coefficient of restitution as $\varepsilon = -V_R/V_T$ (see figure 4). Another option is to define the effective coefficient of restitution by using V_C instead of V_T. In general, the measurement of the velocity just prior to impact is difficult since the effective contact time can be significantly smaller than the temporal resolution of the measurement apparatus (see Joseph *et al.* 2001; Gondret *et al.* 2002, for instance). In the same way, the velocity just prior to impact may vary with the numerical time step used in numerical simulations, especially if the fluid time step is larger than the contact time. In most of the numerical studies, the velocity V_T is therefore used as the velocity prior to contact (see e.g. table 3). The same definition has been used in the present study. In experiments, the measured velocity prior to contact might lie in the range $[V_C \; V_T]$. With this in mind, Ardekani & Rangel (2008) used both V_T and a velocity just prior to impact in the interval $[V_C, V_T]$ and did not show significant modification of the evolution of the coefficient of restitution as a function of St (see figure 6*b*). Here, we observed that the relative variation $(V_T - V_C)/V_T$ was in the range

	ρ_p/ρ	Re_p	η_e/R	$D/\Delta x$	Δ_{lub}	St	$\varepsilon/\varepsilon_{max}$	Comments
◇	8	[0.1, 158]	2×10^{-4}	20	$R/2$	[0.1, 149]	[0, 0.85]	Reference
∗	[8, 900]	≈ 1	2×10^{-4}	20	$R/2$	[1, 100]	[0, 0.73]	Effect of Re_p
■	[7, 90]	≈ 10	2×10^{-4}	20	$R/2$	[8, 86]	[0, 0.84]	
▼	[4, 90]	≈ 100	2×10^{-4}	20	$R/2$	[60, 1090]	[0.59, 0.98]	
★	8	58	2×10^{-4}	20	R	55	0.63	Effect of Δ_{lub}
	8	[8, 158]	2×10^{-4}	20	Δx	[8, 149]	[0, 0.87]	
▲	1.7	[7, 163]	2×10^{-4}	20	$R/2$	[1.7, 41.8]	[0, 0.11]	Effect of ρ_p/ρ
△	2.5	[58, 140]	2×10^{-4}	20	$R/2$	[19, 47]	[0, 0.42]	
▼	[4, 22]	[121, 73]	2×10^{-4}	20	$R/2$	[60, 183]	[0.59, 0.9]	
+	32	[0.6, 98]	2×10^{-4}	20	$R/2$	[2, 354]	[0, 0.95]	
●	8	58	10^{-5}	20	$R/2$	55	0.59	Effect of η_e/R
○	8	58	10^{-3}	20	$R/2$	55	0.67	
▶	8	46	2×10^{-4}	10	$R/2$	49	0.58	Effect of $D/\Delta x$
◀	8	54	2×10^{-4}	40	$R/2$	51	0.62	

TABLE 2. Parameters used in the simulations of figure 6, namely the density ratio ρ_p/ρ, particle Reynolds number Re_p, effective roughness height η_e/R, grid resolution $D/\Delta x$, distance Δ_{lub} of application of the lubrication force (2.18).

1–20 % in cases where rebound occurred. For instance, in the configuration $\rho_p/\rho = 8$, $(V_T - V_C)/V_T \approx 5$ %, 12 % and 20 % at $St = 149$, 54 and 21. This would lead to variations of the normal coefficient of restitution of approximately 20 % in the region of Stokes numbers $10 \leqslant St \leqslant 100$. This variation is in fact within the dispersion range of the experimental data (see figure 6a). Therefore, it is reasonable to use the present definition for the coefficient of restitution.

Values of $\varepsilon/\varepsilon_{max}$ obtained from the simulations without any lubrication model are reported in figure 5 as a function of St. For comparison, we include available experimental data obtained for the rebound of spherical particles, drops or balloons from a wall (table 1). While the numerical results are in good agreement with experiments for $St \geqslant 200$, the effective coefficient of restitution is clearly overestimated at lower St. This is attributed to the low spatial resolution of the flow field when the gap between the particle and the wall is of the order of the grid size. As a consequence, the film pressure stemming from the drainage of the liquid in the gap is underestimated so the particle rebound is artificially enhanced.

This issue is overcome when one adds a lubrication force (2.18) in (2.7). Figure 6(a) shows the results obtained with the present method when the lubrication model is activated for various ρ_p/ρ and Re_p. The numerical results fall within the range of the experimental data. The use of (2.18) allows the method to reproduce the rebound of a particle in a viscous fluid as the lubrication model compensates the inability of the flow solver to capture the small-scale flow field in the gap during the film drainage. We shall demonstrate in the next section that using (2.18) is critical, with the present method, to accurately capture the velocity of approach of the particle at a very small distance from the wall, typically a few per cent of the particle radius. Note that the present implementation of the lubrication force (2.18) gives good results with the present spatial resolution and physical parameters; however it may not be relevant otherwise, in particular when a very fine grid resolution is used.

	Reference	u'	u''	Stokes number
▷	Ardekani & Rangel (2008)	V_T	$\boldsymbol{u}_p(t_{cont} + 0.001\ \text{s})$	$(\rho_p + C_M\rho)V_T D/(9\mu)$
◁	Ardekani & Rangel (2008)	V_C	$\boldsymbol{u}_p(t_{cont} + 0.001\ \text{s})$	$\rho_p V_T D/(9\mu)$
▽	Breugem (2010)	V_T	V_R	$\rho_p V_C D/(9\mu)$
△	Brändle de Motta *et al.* (2013)	V_T	V_R	$\rho_p V_C D/(9\mu)$
◇	Kempe & Fröhlich (2012)†	V_T	$\boldsymbol{u}_p(\boldsymbol{x}_p = \xi_{n,0})$ with $\xi_{n,0} = \boldsymbol{x}_p(\boldsymbol{u}_p = u')$	$\rho_p V_C D/(9\mu)$
□	Li *et al.* (2012)	Not given	Not given	$\rho_p V_C D/(9\mu)$
●	Present study	V_T	V_R	$(\rho_p + C_M\rho)V_T D/(9\mu)$

TABLE 3. Parameters used for the definition of the effective coefficient of normal restitution, here defined as $(u''/u')/\varepsilon_{max}$ with ε_{max} being the coefficient of restitution for a dry collision, and the Stokes number reported in figure 6(*b*). We use the notation V_C and V_R when the authors report the velocity just prior to and just after contact, respectively. t_{cont} is the time instant at which contact occurs. † In Kempe & Fröhlich (2012), $\xi_{n,0}$ is the particle–wall distance chosen large enough to neglect hydrodynamic interaction of the particle with the wall.

Figure 6(*a*) also shows the sensitivity of the numerical model to the different parameters. In particular, the relative roughness height, the distance of activation of the lubrication force, the grid resolution are varied and it is shown that simulations fall within the range of the experimental data which underlines the robustness of our numerical model. Finally, investigation of several density ratios and Reynolds numbers shows a good agreement with experiments.

We compare in figure 6(*b*) the present results with those obtained with other numerical methods (see table 3) using either a different fixed-grid approach or a different model to handle small-scale interactions (lubrication, solid–solid contact). Table 3 reports the various definitions used for the velocity just prior to impact, the subsequent coefficient of restitution, and the Stokes number. The numerical results all fall in the same range, in reasonable agreement with experimental data. This gives further support that the present definitions for the Stokes number and restitution coefficient are relevant for this problem.

3.2. *Small-scale dynamics of a sphere approaching a wall*

Mongruel *et al.* (2010) investigated experimentally the dynamics of a sphere settling in a fluid toward a wall at a sufficiently low Stokes number so that no bouncing was observed. They measured with an interferometric device the position and velocity of the particle up to a small distance from the wall, typically in the range of a few per cent of the particle radius. In their experiments, Mongruel *et al.* (2010) used millimetric steel balls in various viscous fluids. The results revealed two regimes which are characterized by a nonlinear dependence of the velocity on the distance to the wall followed by a linear dependence just prior to contact (see figure 7 for instance). The experimental measurement of the transition height delimiting these two regimes was found in the range 0.1–6% of R for particles of radius in the range 2.7–7 mm. Moreover, Mongruel *et al.* (2010) proposed a model based on a second-order ordinary differential equation describing the temporal evolution of the
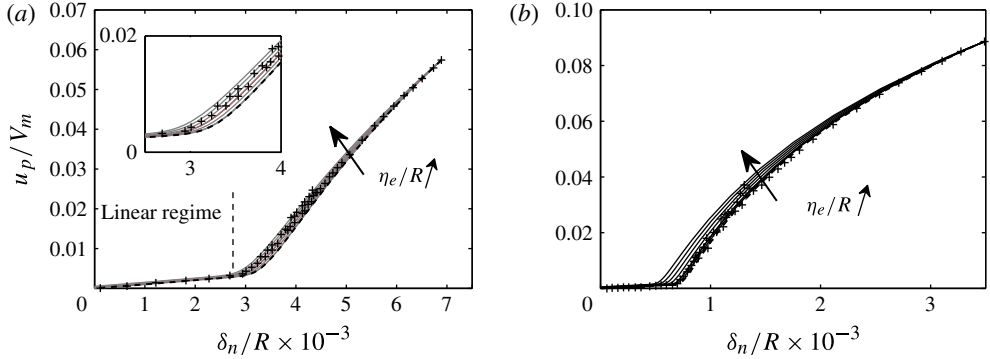
FIGURE 7. (Colour online) Dimensionless velocity u_p/V_m as a function of the dimensionless length δ_n/R: +, experiments of Mongruel *et al.* (2010); ——, analytical solutions of (3.2) with various relative roughness heights $5 \times 10^{-5} \leqslant \eta_e/R \leqslant 5 \times 10^{-4}$ (the dashed line corresponds to $\eta_e = 0$ as derived in Mongruel *et al.* 2010). (*a*) $V_m = 0.77$ m s^{-1} and $St_m = 10.9$; (*b*) $V_m = 0.98$ m s^{-1} and $St_m = 15.96$. Inset: close-up view of the transition region separating the linear and nonlinear regimes.

particle–wall distance δ_n, assuming that lubrication is the dominant effect. Following Mongruel *et al.* (2010), we propose a modified version of their equation (3.4) using the lubrication force (2.18) in which the effective roughness height of the particle η_e is considered. Assuming $\delta_n/R \ll 1$ and the lubrication force (2.18) to be the dominant hydrodynamic force, the evolution of the normalized particle–wall distance δ_n/R can then be written as

$$-St_m \frac{\mathrm{d}^2 \delta_n/R}{\mathrm{d}\tau^2} = \frac{R}{\delta_n + \eta_e} \frac{\mathrm{d}\delta_n/R}{\mathrm{d}\tau} + 1, \qquad (3.2)$$

where $St_m = \rho_p V_m^2/(\rho_p - \rho)gR$ is a modified Stokes number representative of particle inertia in the near-wall region, V_m is a characteristic velocity of the particle and $\tau = tV_m/R$. The value of V_m is measured *a posteriori* from experimental data in the linear regime (see figure 7) via the relation $u_p/V_m = \delta_n/R$ ((3.2) of Mongruel *et al.* 2010). Figure 7 shows the dimensionless velocity u_p/V_m of the particle approaching the wall as a function of δ_n/R, in which both the experimental data of Mongruel *et al.* (2010) and the solution of (3.2) for various relative effective roughness heights $5 \times 10^{-5} \leqslant \eta_e/R \leqslant 5 \times 10^{-4}$ are shown. The model (3.2) is shown to quantitatively reproduce the observed dynamics of the particle and in particular the transition height between the two regimes. More precisely, the variation of the model's solution with respect to the effective roughness height of the particle coincides with the dispersion of the experimental data when δ_n gets closer to the transition between the two regimes.

In the following, we reproduce the experiments of Mongruel *et al.* (2010) for which a steel sphere ($\rho_p = 7800$ kg m^{-3}, $\mu_p = 0.2$, $\varepsilon_{max} = 0.97$, $R = [4; 5.25; 6.35; 7$ mm]) settles in silicon oil ($\rho = 978$ kg m^{-3}, $\mu = 0.978$ kg m^{-1} s^{-1}) using the present numerical approach with the resolution and geometry used in §3.1. We chose $\eta_e/R = 2 \times 10^{-4}$, which corresponds to the best fit of the experimental data in figure 7 using model (3.2). In the numerical simulation, the sphere is initially released 40 cm above the horizontal wall. Figure 8 shows the results for the dimensionless velocity u_p/V_m as a function of δ_n/R. Simulation results are in good agreement with experimental data. For instance, in the case reported in figure 8(*b*), the values of V_m and St_m obtained in the numerical simulation (experiments) are $V_m = 0.74$ m s^{-1}
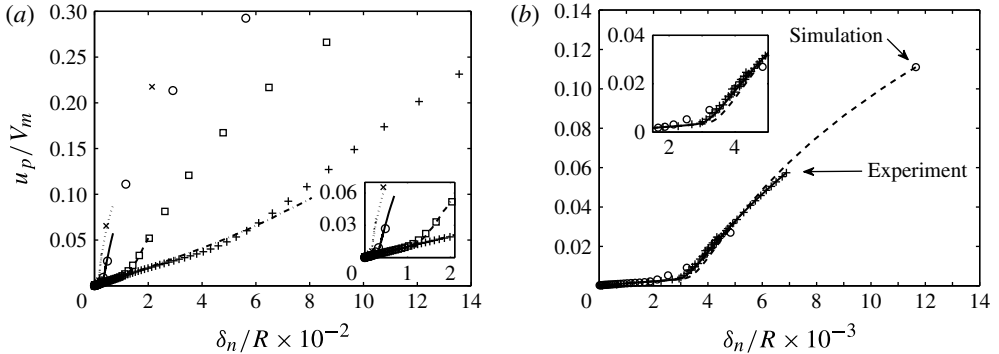
FIGURE 8. Velocity of a sphere approaching a wall as a function of the wall–sphere distance. (*a*) Experiments of Mongruel *et al.* (2010): - · - · - ·, $V_m = 0.28$ m s^{-1}, $St_m = 2.3$; - - - -, $V_m = 0.51$ m s^{-1}, $St_m = 5.7$; ———, $V_m = 0.77$ m s^{-1}, $St_m = 10.9$; (· · · · · ·) $V_m = 0.98$ m s^{-1}, $St_m = 15.9$. Present simulations: +, $V_m = 0.48$ m s^{-1}, $St_m = 3.9$; □, $V_m = 0.62$ m s^{-1}, $St_m = 6.4$; ○, $V_m = 0.74$ m s^{-1}, $St_m = 9.3$; ×, $V_m = 0.81$ m s^{-1}, $St_m = 10.9$. (*b*) +, Experimental data of Mongruel *et al.* (2010) ($V_m = 0.77$ m s^{-1}, $St_m = 10.9$); ○, present simulation ($V_m = 0.74$ m s^{-1}, $St_m = 9.3$). For comparison, dashed and solid lines are the solution of (3.2) using as initial condition the distance and velocity of the particle at times corresponding to the points highlighted by an arrow for the simulation and the experiment, respectively. The effective roughness height for the simulation was set to $\eta_e/R = 2 \times 10^{-4}$. Insets: close-up view near the transition between the linear and nonlinear regimes.

(0.77) and $St_m = 9.3$ (10.9). The discrepancy is due to a slight difference, within 4 %, in the steady settling velocity far from the wall. Solutions of the model (3.2) are also presented in figure 8(*b*). Again, quantitative agreement is obtained between the different methods with a maximum of the error at the transition between the two regimes.

3.3. *A new model for the prediction of the effective coefficient of restitution*

In this section, we propose a new model predicting the effective coefficient of restitution $\varepsilon = -V_R/V_T$. As shown later, this model only depends on two parameters, namely the Stokes number (3.1) and the relative effective roughness height η_e/R. Some recent attempts have been made to predict the coefficient of restitution using models based either on lubrication theory (elasto-hydrodynamics model, Davis *et al.* 1986; Barnocky & Davis 1988; mixed contact model, Yang & Hunt 2008), or on a mass–spring analogy (Legendre *et al.* 2005, 2006). Solving the equations of motion for a spherical particle approaching a wall, and assuming lubrication force to be dominant (see e.g. (3.5) and (3.6) below), it is possible to obtain a model of effective coefficient of restitution (see (2.3) in Yang & Hunt 2008), as

$$\frac{\varepsilon}{\varepsilon_{max}} = 1 + \frac{\kappa}{St} \ln \left(\frac{\eta}{R} \right), \tag{3.3}$$

where κ is a constant of $O(1)$ and η is the mean height of surface asperities of the sphere. Yang & Hunt (2008) extended the model (3.3) in order to account for the viscous dissipation occurring in the liquid wells trapped between the asperities during

the contact. The mixed-contact model is written

$$\frac{\varepsilon}{\varepsilon_{max}} = \sigma + \frac{1/\varepsilon_{max} + \sigma}{St} \ln\left(\frac{\delta_f}{\delta_0}\right), \qquad (3.4)$$

where $0 \leqslant \sigma \leqslant 1$ is a coefficient which depends on a critical Stokes number St_c below which there is no bouncing, as $\sigma = 1 - St_c/St$, δ_f is the minimum approach distance of the particle during the collision, and δ_0 is a characteristic distance at which deformation of the sphere due to lubrication effects occurs. In their paper, Yang & Hunt (2008) reported values of St_c and δ_f/δ_0 in the range [5, 20] and [10^{-4}, 10^{-2}], respectively.

Legendre *et al.* (2005) performed experiments with light drops rising in a liquid and bouncing on a wall. They modelled the possible rebound of the inclusion using an analogy with a dissipative mass–spring system. They obtained the expression $\varepsilon/\varepsilon_{max} = \exp(-\chi/St)$ with χ a parameter which includes the viscous effects of the film drainage. According to their experiments, the original value of χ was estimated to be a constant $\chi \approx 14$. However, it appeared that quantitative agreement with other types of inclusion was found for $\chi \approx 35$.

The above-mentioned models are compared to experimental data in figure 5. In models (3.3) and (3.4) we have set $\kappa = 1$, $\eta/R = 10^{-4}$, and $\varepsilon_{max} = 0.97$, $St_c = 20$, $\delta_f/\delta_0 = 10^{-3}$, respectively, which are in the range of values reported in Yang & Hunt (2008). The models (3.3) and (3.4), which are based on lubrication theory, quantitatively reproduce experimental observation in some specific ranges of St. However, they are not able to predict the effective coefficient of restitution for the whole range of Stokes number. Conversely, Legendre *et al.* (2005)'s model is in good agreement with experiments; however recall that it makes use of an adjusted constant.

Here we revisit both types of theory to derive a simple model which is able to capture reasonably well the observed effective coefficient of restitution for the whole range of Stokes number considered here (see figure 10 below). First, it can be noted that for large Stokes number, $St \gg 1$, the bouncing is similar to dry configurations. In this regime, lubrication acts on a length scale that is small compared to the effective roughness height of the particle. On the other hand, at relatively small Stokes number, $St \leqslant O(10)$, no bouncing occurs. Lubrication is dominant and dissipates the initial kinetic energy of the particle before it reaches the wall. In the intermediate regime, bouncing occurs but is largely affected by the surrounding fluid, as observed in figure 5. In the following model, the influence of this surrounding fluid is considered by introducing a lubrication component into two distinct stages.

The first stage starts from a characteristic time at which the particle velocity begins to be influenced by the wall (i.e. for $\delta_n \approx R$, approximately, see figures 3 and 4 and corresponding discussions) up to the time at which collision occurs ($\delta_n = 0$). During this stage, the particle is assumed (i) not to be deformed and (ii) to be affected by viscous forces generated by the displacement of fluid due to the presence of the wall. On such a length scale, $O(R)$, lubrication is therefore supposed to act only through dissipation of the kinetic energy but not to deform the particle. During the first stage, the particle velocity decreases from V_T to V_C (see figure 4 for definition). In the second stage, however, the particle gets deformed and bounces. During this stage, we assume that the particle kinetic energy is converted into energy of elastic deformation and is only partially restored into kinetic energy because some of the energy has been dissipated by both inelastic deformation and viscous dissipation. During the rebound, lubrication still occurs due to the drainage of the fluid on the length scale of the
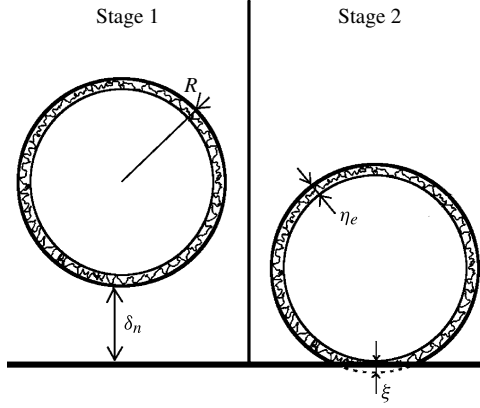
FIGURE 9. Sketch of the bouncing of a particle split into two distinct stages as assumed in the model derived in § 3.3: δ_n is the particle–wall distance; η_e is the effective roughness height of the sphere and ξ is the deformation of the particle during contact. Deformation is assumed to take place only during stage 2 ($\delta_n = 0$).

effective roughness height η_e. One of the specific aspects of the present model is then to consider that the elastic stress related to the deformation of the particle during bouncing and the pressure induced by the lubricating fluid film are of the same order of magnitude. This assumption is not straightforward and will be elaborated at the end of this section. During the second stage, the particle velocity goes from V_C to V_R.

In order to estimate the ratio V_C/V_T, we consider that the particle, at centroid location x_p and of velocity $\boldsymbol{u}_p = u_p \boldsymbol{n}$, is moving toward a flat wall in a fluid at rest and we assume that the particle is subject to a steady drag force which is balanced by the buoyancy force, the added-mass force and the lubrication force $\boldsymbol{F}_{lub} = F_{lub} \boldsymbol{n}$ defined in (2.18) which, in the present case, becomes $F_{lub} = -6\pi\mu u_p R^2/(\delta_n + \eta_e)$. The kinematic equations then become,

$$\frac{\mathrm{d}x_p}{\mathrm{d}t} = -u_p, \tag{3.5}$$

$$(m_p + C_M m)\frac{\mathrm{d}u_p}{\mathrm{d}t} = F_{lub}, \tag{3.6}$$

where m is the mass of the fluid contained in a sphere of radius R and $C_M = 1/2$ is the added-mass coefficient. Note that, strictly speaking, the added-mass coefficient C_M changes as the particle gets closer to the wall (see e.g. the discussion in Legendre et al. 2005). In practice, C_M is increased from 0.5 to 0.7 approximately when the particle is very close to the wall. Here, however, we keep $C_M = 1/2$ for simplicity. Using the relation $x_p = R + \delta_n$, then dividing (3.6) by (3.5) in order to eliminate time, and integrating between $\delta_n = 0$ ($u_p = V_C$) and $\delta_n = R$ ($u_p = V_T$), we find the ratio $\beta \equiv V_C/V_T$, namely

$$\beta \equiv \frac{V_C}{V_T} = 1 + \frac{1}{St} \ln\left(\frac{\eta_e}{R}\right), \tag{3.7}$$

where we assumed that $R \gg \eta_e$. Equation (3.7) is similar to the relation given by Davis et al. (1986).

Regarding the second stage, we follow Legendre et al. (2005)'s analysis and use a mass–spring model to describe the deformation ξ of the particle (see figure 9) where

we take into account energy loss due inelastic deformation and viscous dissipation. Here, the deformation force is considered to be linear with ξ and hence does not follow the Hertzian model for simplicity. This is in line with the collision model used for our simulations. The deformation of the particle is then governed by

$$(m_p + C_M m)\frac{\mathrm{d}^2\xi}{\mathrm{d}t^2} + (6\pi\mu R^2/\eta_e + \gamma_n)\frac{\mathrm{d}\xi}{\mathrm{d}t} + k_n\xi = 0, \tag{3.8}$$

with initial conditions $\xi = 0$ and $\mathrm{d}\xi/\mathrm{d}t = V_C$ when the particle impacts on the wall. Recall that γ_n and k_n are the damping and stiffness coefficient of the soft-sphere mass–spring model, respectively. Here the lubrication damping term in (3.8) is inversely proportional to the relative roughness height of the particle. Strictly speaking, this term could vary during impact if the fluid film thickness between the two solids varies. We assume here that this length remains of the same order during impact implying that the lubrication force only evolves with the velocity due to the deformation of the particle during impact, as also assumed in the model developed by Legendre *et al.* (2005). Integrating (3.8) with the corresponding initial conditions gives the classical solution $\xi(t)$ of a damped harmonic oscillator (not shown), then using the definitions $\mathrm{d}\xi(t_{cont})/\mathrm{d}t = V_C$ (at the time of contact t_{cont}) and $\mathrm{d}\xi(t_{cont} + \tau)/\mathrm{d}t = V_R$ (at the time of rebound) gives

$$V_R = -V_C \exp\left(-\frac{\lambda\tau}{2m^*}\right), \tag{3.9}$$

with τ being the half-period of oscillation

$$\tau = \pi\frac{\sqrt{m^*/k_n}}{\sqrt{1 - \lambda^2/4k_n m^*}}, \tag{3.10}$$

and where $m^* = m_p + C_M m$ and $\lambda = 6\pi\mu R^2/\eta_e + \gamma_n$. Equation (3.10) indicates that the larger the viscosity and/or γ_n, the larger τ, so that the contact time is larger accordingly, as expected. However, recent experiments on the impact of a solid sphere on a wall showed that the effective contact time remains finite and of the order of the contact time predicted by Hertz theory (considering no interaction with the surrounding fluid), in a large range of Stokes number $20 \leqslant St \leqslant 10^3$ (Legendre *et al.* 2006). Therefore, it is reasonable to approximate (3.10) by $\tau = \pi\sqrt{m^*/k_n}$. Moreover, we further assume a balance between elastic stress of deformation and lubrication pressure induced by the fluid film on the effective roughness height which gives $R/\eta_e \approx \sqrt{k_n/6\pi\mu V_C}$. The implications of the above assumptions are discussed at the end of the section. Using this together with (3.9) and the approximation $\tau = \pi\sqrt{m^*/k_n}$, we obtain an expression for the rebound velocity V_R, as a function of the contact velocity V_C,

$$\frac{V_R}{V_C} = -\varepsilon_{max}\exp\left(-\frac{\pi/2}{\sqrt{\beta St}}\right), \tag{3.11}$$

where β is a parameter defined in (3.7) which depends on the Stokes number and the effective roughness height. Note that (3.11) implies that $\beta > 0$ so that β varies in the range $]0, 1]$. Combining (3.7) and (3.11), we find a new model for the prediction of the normalized effective coefficient of restitution for a colliding solid sphere in a viscous fluid,

$$\frac{\varepsilon}{\varepsilon_{max}} = \frac{-V_R/V_T}{\varepsilon_{max}} = \beta\exp\left(-\frac{\pi/2}{\sqrt{\beta St}}\right). \tag{3.12}$$
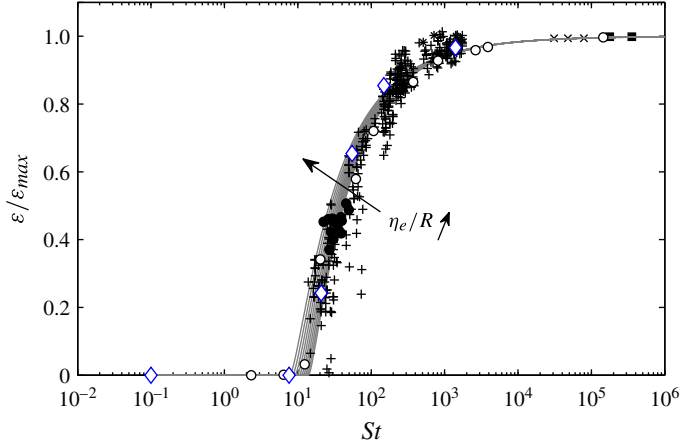
FIGURE 10. (Colour online) Same as figure 5 but with new model added. $\Diamond$, Present simulations with lubrication force (2.18) for $\rho_p/\rho = 8$, $\eta_e/R = 2 \times 10^{-4}$. Experiments: other symbols, see table 2 for key. ——, Model (3.12) with various relative roughness heights $10^{-6} \leqslant \eta_e/R \leqslant 10^{-3}$: η_e/R increases from the lower curve to the upper curve.

As mentioned above, this new model only depends on two parameters, namely St and η_e/R (via β). Note that here no adjustable constant was used. The model (3.12) is plotted in figure 10 for a range of relative roughness heights $10^{-6} \leqslant \eta_e/R \leqslant 10^{-3}$. Good agreement is observed for both small and large values of the Stokes number. Note that the sensitivity of (3.12) with respect to η_e/R is larger at moderate-to-small Stokes numbers. This is in line with the dispersion of experimental results which is observed to be larger at low St. Furthermore, as has been observed numerically by Ardekani & Rangel (2008), (3.12) verifies that the effect of the roughness decreases with increasing Stokes number.

Note that (3.12) can be rewritten as a function of the critical Stokes number St_c below which there is no bouncing. Taking $\varepsilon = 0$ and using (3.7), one finds a relation between St_c and η_e, namely $St_c = \ln(R/\eta_e)$. Using this relation with the range of η_e/R reported in figure 10 gives $7 \leqslant St_c \leqslant 14$, in reasonable agreement with the range $5 \leqslant St_c \leqslant 20$ reported in experiments (Joseph *et al.* 2001; Gondret *et al.* 2002). However, it must be stressed that η_e is an effective roughness height accounting for the mean height of surface asperities of real particles η. A detailed investigation of the relation between these parameters would require a specific study which is beyond the scope of the present work. Finally, using this definition of St_c, (3.7) can be equivalently written as $\beta = (St - St_c)/St$, and one can thus express $\varepsilon/\varepsilon_{max}$ as a function of St_c from (3.12), namely

$$\frac{\varepsilon}{\varepsilon_{max}} = \left(1 - \frac{St_c}{St} \right) \exp\left(-\frac{\pi/2}{\sqrt{St - St_c}} \right). \qquad (3.13)$$

As already mentioned, the model (3.12) has been obtained by assuming (i) the contact time τ only depends on elastic parameters and not on solid and viscous dissipations and (ii) $R/\eta_e \sim \sqrt{k_n/6\pi\mu V_C}$, i.e. the elastic stress balances the pressure induced by the lubricating film. Note that the aim of simplifications associated with these assumptions is to derive a simple predictive model which can reproduce the coefficient of restitution for a large range of St and with a minimum set of non-dimensional numbers. As a result, the normalized solution (3.12) is only a

function of β and St and does not depend on the elastic properties of the particle. Note that the solid dissipation associated with the deformation of the particle during contact is accounted for in ε_{max} used to scale ε. We have already discussed assumption (i). Assumption (ii), however, needs some discussion. In particular, two other extreme cases could have been considered to model bouncing. A first one is to assume that lubrication effects are important enough to induce elastic deformation of the particle prior to any solid contact.

This situation has been treated by Davis *et al.* (1986) for smooth particles. In this specific case, they show that the restitution is again strongly related to St and, to a lesser extent, to a so-called elasticity parameter which includes among other things the elastic properties of the particle. This configuration cannot be captured by the present model since (3.8) assumed no deformation of the particle prior to solid contact. Davis *et al.* (1986)'s solution proved to be pertinent at small St and for smooth particles. On the other hand, it is not at present clear how this solution holds for rough particles and larger St, and therefore able to describe the experimental data reported in the literature and discussed here. Once again, the choice made here is to consider that roughness effects prevail over elasto-hydrodynamic deformations.

The other extreme case would be to suppose that the lubrication pressure remains small compared to the elastic stress during solid bouncing. In that case, the solid dissipation can be considered as dominant over the fluid dissipation on the time scale of the solid contact, and therefore $\lambda = \gamma_n$. This would lead to a modification of the exp term in (3.12) which would be close to unity and therefore $\varepsilon/\varepsilon_{max} = \beta$. As this solution slightly overestimates the experimental and numerical data, the new model (3.12) is therefore preferred to predict the effective coefficient of restitution of the particle bouncing in a viscous fluid.

3.4. *A note on the critical distance of influence of the wall*

As mentioned earlier, Joseph *et al.* (2001) measured in their experiments the critical distance h_w at which the velocity of the particle decreases due to the presence of the wall, and found $0 \leqslant h_w \leqslant R$ for $9 \leqslant St \leqslant 70$. Above this distance, there is no wall effect on the particle which is moving steadily, the drag force balancing the buoyancy force. The wall effect implies a modification of hydrodynamic forces in the system leading to unsteady motion of the particle. Cox & Brenner (1967) show that, at moderate Reynolds number, the correction scales as $1/h$ with h being the distance from the wall, here $h = \delta_n + \eta_e \sim \delta_n$ at leading-order. Even if an inertial correction can be added to this solution (Cox & Brenner 1967), we focus here on the dominant wall effect associated with the leading-order correction. The expansion is shown to be consistent with the lubrication theory. Therefore, in non-dimensional form, a small deviation from steady equilibrium induced by the wall is dictated by a balance between inertia and modified drag (or equivalently lubrication force), i.e.

$$St\frac{\mathrm{d}\tilde{u}_p}{\mathrm{d}\tilde{t}} \sim \frac{\tilde{u}_p}{\tilde{h}}, \tag{3.14}$$

where the tilde refers to dimensionless quantities using V_T and R as the velocity and length scales respectively. Defining the critical distance h_w as the distance from which the particle starts to decelerate, a natural scaling emerges from (3.14)
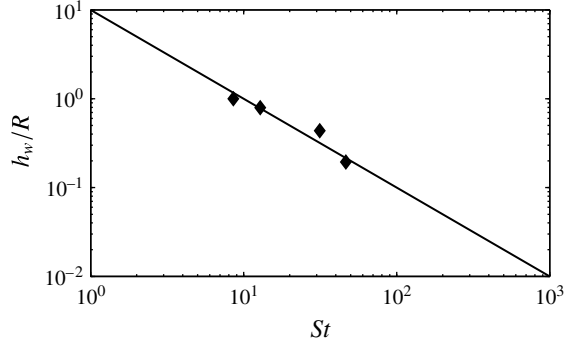
$$\frac{h_w}{R} \sim \frac{1}{St}. \tag{3.15}$$

FIGURE 11. Critical distance h_w of influence of the wall as a function of the Stokes number: ♦, experiments of Joseph *et al.* (2001); ——, best fit using model (3.15).

The model (3.15) is compared to the experimental measurements of Joseph *et al.* (2001) in figure 11. A good agreement is observed, giving further support that h_w scales as St^{-1}.

4. Conclusion

A simple soft-sphere IBM has been developed and used to quantitatively reproduce experimental observations of the dynamics of a solid particle bouncing on a horizontal wall in a viscous fluid. The proposed numerical method is based on two different time steps considering that solid contact occurs on a time scale that is much smaller than the fluid one. Simulations are shown to be in good agreement with available experimental results as well as other numerical models available in the literature, for the whole range of investigated parameters, provided that a local lubrication model is used including an effective roughness height modelling the roughness of real particle surfaces. Also, two models, accounting for the effective roughness length, have been proposed here to describe a regime in which the solid particle can stick to the wall (small Stokes number, i.e. $St < 10$) and a regime characterized by a bounce of the particle ($St > 10$).

In the first regime, $St < 10$, the numerical results show that this type of fixed-grid approach is able to accurately reproduce the approach of a sphere toward a wall, even at a very small distance from the wall, i.e. less than a few per cent of the sphere radius. This specific case is considered as a demanding test to validate the lubrication force implemented in the numerical model. Moreover, the analytic model, extended from Mongruel *et al.* (2010), shows that the implementation of the roughness length allows one to predict more accurately the dynamics of the particle approaching the wall. In the second regime, $St > 10$, the bouncing is characterized by an effective coefficient of restitution which tends to the solid one for large St as already observed in numerous experimental and numerical studies. The numerical method is shown here to predict reasonably well this coefficient of restitution within the range of dispersion of experimental and numerical results. The proposed restitution model allows the reproduction of the coefficient of normal restitution observed in experiments and numerical studies, with no adjustable constant. Moreover, the present results support the experimental observation that the particle roughness could be responsible for the variance of effective restitution when St decreases to St_c (see e.g. Joseph *et al.* 2001).

The numerical model used in this study can be easily extended to more complex systems. It will be used in a future work to describe and characterize large-scale dynamics of multiple interacting particles in dense packing configurations.

Acknowledgements

REFERENCES

ARDEKANI, A. M. & RANGEL, R. H. 2008 Numerical investigation of particle–particle and particle–wall collisions in a viscous fluid. *J. Fluid Mech.* **596**, 437–466.

BARNOCKY, G. & DAVIS, R. H. 1988 Elastohydrodynamic collision and rebound of spheres: experimental verification. *Phys. Fluids* **31**, 1324–1329.

BARNOCKY, G. & DAVIS, R. H. 1989 The influence of pressure-dependent density and viscosity on the elastohydrodynamic collision and rebound of two spheres. *J. Fluid Mech.* **209**, 501–519.

BIGOT, B., BONOMETTI, T., LACAZE, L. & THUAL, O. 2013 A simple immersed-boundary method for solid–fluid interaction in constant- and stratified-density flows. *Comput. Fluids*, doi:10.1016/j.compfluid.2014.03.030.

BRÄNDLE DE MOTTA, J. C., BREUGEM, W.-P., GAZANION, B., ESTIVALEZES, J.-L., VINCENT, S. & CLIMENT, E. 2013 Numerical modelling of finite-size particle collisions in a viscous fluid. *Phys. Fluids* **25**, 083302.

BRENNER, H. 1961 The slow motion of a sphere through a viscous fluid towards a plane surface. *Chem. Engng Sci.* **16**, 242–251.

BREUGEM, W.-P. 2010 A combined soft-sphere collision/immersed boundary method for resolved simulations of particulate flows. *Proceedings of the ASME FED SM* 2010 30634.

BREUGEM, W.-P. 2012 A second-order accurate immersed boundary method for fully resolved simulations of particle-laden flows. *J. Comput. Phys.* **231**, 4469–4498.

COX, R. G. & BRENNER, H. 1967 The slow motion of a sphere through a viscous fluid towards a plane surface–II small gap widths, including inertial effects. *Chem. Engng Sci.* **22**, 1753–1777.

CUNDALL, P. A. & STRACK, O. D. L. 1979 A discrete numerical model for granular assemblies. *Gèotechnique* **29**, 47–65.

DAVIS, R. H. 1987 Elastohydrodynamic collisions of particles. *Physico-Chem. Hydrodyn.* **9**, 41–52.

DAVIS, R. H., SERAYSSOL, J.-M. & HINCH, E. J. 1986 Elastohydrodynamic collision of two spheres. *J. Fluid Mech.* **163**, 479–497.

FABRE, D., TCHOUFAG, J. & MAGNAUDET, J. 2012 The steady oblique path of buoyancy-driven disks and spheres. *J. Fluid Mech.* **707**, 24–36.

FADLUN, E. A., VERZICCO, R., ORLANDI, P. & MOHD-YUSOF, J. 2000 Combined immersed-boundary finite-difference methods for three-dimensional complex flow simulations. *J. Comput. Phys.* **161**, 35–60.

FENG, Z. G., MICHAELIDES, E. E. & MAO, S. 2010 A three-dimensional resolved discrete particle method for studying particle-wall collision in a viscous fluid. *J. Comput. Phys.* **161**, 35–60.

FOERSTER, S. F., LOUGE, M. Y., CHANG, H. & ALLIA, K. 1994 Measurements of the collision properties of small spheres. *Phys. Fluids* **6**, 1108–1115.

GONDRET, P., LANCE, M. & PETIT, L. 2002 Bouncing motion of spherical particles in fluids. *Phys. Fluids* **14**, 643–652.

JENNY, M., DUSEK, J. & BOUCHET, G. 2004 Instabilities and transition of a sphere falling or ascending freely in a Newtonian fluid. *J. Fluid Mech.* **508**, 201–239.

JOSEPH, G. G. & HUNT, M. L. 2004 Oblique particle-wall collisions in a liquid. *J. Fluid Mech.* **510**, 71–93.

JOSEPH, G. G., ZENIT, R., HUNT, M. L. & ROSENWINKEL, A. M. 2001 Particle-wall collisions in a viscous fluid. *J. Fluid Mech.* **433**, 329–346.

KEMPE, T. & FRÖHLICH, J. 2012 Collision modelling for the interface-resolved simulation of spherical particles in viscous fluids. *J. Fluid Mech.* **709**, 445–489.

KIM, J., KIM, D. & CHOI, H. 2001 An immersed-boundary finite-volume method for simulations of flow in complex geometries. *J. Comput. Phys.* **171**, 132–150.

LACAZE, L., PHILLIPS, J. C. & KERSWELL, R. R. 2008 Planar collapse of a granular column: experiments and discrete element simulations. *Phys. Fluids* **20**, 063302.

LECOQ, N., ANTHORE, R., CICHOCKI, B., SZYMCZAK, P. & FEUILLEBOIS, F. 2004 Drag force on a sphere moving towards a corrugated wall. *J. Fluid Mech.* **513**, 247–264.

LEGENDRE, D., DANIEL, C. & GUIRAUD, P. 2005 Experimental study of a drop bouncing on a wall in a liquid. *Phys. Fluids* **17**, 097105.

LEGENDRE, D., ZENIT, R., DANIEL, C. & GUIRAUD, P. 2006 A note on the modelling of the bouncing of spherical drops or solid spheres on a wall in viscous fluid. *Chem. Engng Sci.* **61**, 3543–3549.

LI, X., HUNT, M. L. & COLONIUS, T. 2012 A contact model for normal immersed collisions between a particle and a wall. *J. Fluid Mech.* **691**, 123–145.

LIAN, G., ADAMS, M. J. & THORNTON, C. 1996 Elastohydrodynamic collisions of solid spheres. *J. Fluid Mech.* **311**, 141–152.

LUNDBERG, J. & SHEN, H. H. 1992 Collisional restitution dependence on viscosity. *J. Engng Mech. ASCE* **118**, 979–989.

MONGRUEL, A., CHASTEL, T., ASMOLOV, E. S. & VINOGRADOVA, O. I. 2013 Effective hydrodynamic boundary conditions for microtextured surfaces. *Phys. Rev.* E **87**, 011002.

MONGRUEL, A., LAMRIBEN, C., YAHIAOUI, S. & FEUILLEBOIS, F. 2010 The approach of a sphere to a wall at finite Reynolds number. *J. Fluid Mech.* **661**, 229–238.

PESKIN, C. S. 2002 The immersed boundary method. *Acta Numerica* **11**, 479–517.

PIANET, G., TEN CATE, A., DERKSEN, J. J. & ARQUIS, E. 2007 Assessment of the 1-fluid method for dns of particulate flows: sedimentation of a single sphere at moderate to high Reynolds numbers. *Comput. Fluids* **36**, 359–375.

RICHARD, D. & QUÉRÉ, D. 2000 Bouncing water drops. *Europhys. Lett.* **50**, 769–775.

SCHÄFER, J., DIPPEL, S. & WOLF, D. E. 1996 Force schemes in simulations of granular materials. *J. Phys. I France* **6**, 5–20.

SIMEONOV, J. A. & CALANTONI, J. 2012 Modeling mechanical contact and lubrication in direct numerical simulations of colliding particles. *Intl J. Multiphase Flow* **46**, 38–53.

SMART, J. R. & LEIGHTON, D. T. 1989 Measurement of the hydrodynamic surface roughness of noncolloidal spheres. *Phys. Fluids* A **1**, 52–60.

TEN CATE, A., NIEUWSTAD, C. H., DERKSEN, J. J. & VAN DEN AKKER, H. E. A. 2002 Particle imaging velocimetry experiments and lattice-Boltzmann simulations on a single sphere settling under gravity. *Phys. Fluids* **14**, 4012–4025.

THOMPSON, J. F., WARSI, Z. U. A. & MASTIN, C. W. 1985 *Numerical Grid Generation: Foundations and Applications*. Elsevier.

UHLMANN, M. 2005 An immersed boundary method with direct forcing for the simulation of particulate flows. *J. Comput. Phys.* **209**, 448–476.

YANG, F.-L. & HUNT, M. L. 2006 Dynamics of particle–particle collisions in a viscous liquid. *Phys. Fluids* **18**, 121506.

YANG, F.-L. & HUNT, M. L. 2008 A mixed contact model for an immersed collision between two solid surfaces. *Phil. Trans. R. Soc. Lond.* A **366**, 2205–2218.

YUKI, Y., TAKEUCHI, S. & KAJISHIMA, T. 2007 Efficient immersed boundary method for strong interaction problem of arbitrary shape object with the self-induced flow. *J. Fluid Sci. Technol.* **2**, 1–11.